CHIN. PHYS. LETT. Vol. 37, No. 8 (2020) 085201

Temperature Gradient, Toroidal and Ion FLR Effects on Drift-Tearing Modes

Hao Shi(时浩)[1,2,3], Wenlu Zhang(张文禄)[2,4,3,1,5*], Chao Dong(董超)[2,3], Jian Bao(包健)[2,3], Zhihong Lin(林志宏)[6], Jintao Cao(曹金涛)[2,3], and Ding Li(李定)[2,4,3,5]

[1]*School of Physical Sciences, University of Science and Technology of China, Hefei 230026, China*
[2]*Beijing National Laboratory for Condensed Matter Physics and Laboratory of Soft Matter Physics, Institute of Physics, Chinese Academy of Sciences, Beijing 100190, China*
[3]*School of Physical Sciences, University of Chinese Academy of Sciences, Beijing 100049, China*
[4]*Songshan Lake Materials Laboratory, Dongguan 523808, China*
[5]*CAS Center for Excellence in Ultra-intense Laser Science, Shanghai 201800, China*
[6]*Department of Physics and Astronomy, University of California, Irvine, California 92697, USA*

(Received 27 May 2020; accepted 28 June 2020; published online 28 July 2020)

The influences of the temperature gradient and toroidal effects on drift-tearing modes have been studied using the Gyrokinetic Toroidal code. After the thermal force term is introduced into the parallel electron force balance equation, the equilibrium temperature gradient can cause a significant increase in the growth rate of the drift-tearing mode and a broadening of the mode structure. The simulation results show that the toroidal effects increase the growth rate of the drift-tearing mode, and the contours of the perturbation field "squeeze" toward the stronger field side in the poloidal section. Finally, the hybrid model for fluid electrons and kinetic ions has been studied briefly, and the dispersion relation of the drift-tearing mode under the influence of ion finite Larmor radius effects is obtained. Compared with the dispersion relation under the fluid model, a stabilizing effect of the ion finite Larmor radius is observed.

PACS: 52.35.Py, 52.65.Kj, 52.65.Tt, 52.55.Fa DOI: 10.1088/0256-307X/37/8/085201

Tearing modes[1−3] are among the most dangerous magnetohydrodynamic (MHD) instabilities in tokamak plasmas, which will lead to formation of a magnetic island through magnetic reconnection. Control of the magnetic island is one of the key issues for achieving high performance in fusion plasma. The drift-tearing mode[4−7] is one of the extensions of the classical tearing mode[8−10] including diamagnetic effect, when the diamagnetic frequency is comparable to the growth rate of the resistive tearing mode. Its significance lies in the self-consistent kinetic studies of the neoclassical tearing mode (NTM),[11] including the onset and the nonlinear phases of NTM, in particular. The free energy in the equilibrium magnetic field is the driving source of the classical tearing mode, while a cross-field pressure gradient serves as an additional energy source in exciting drift-tearing instabilities.

The influence of the equilibrium density gradient was considered previously in our simulation study of the drift-tearing mode.[12] The results showed that the coupling of drift modes to tearing modes led to a substantial reduction in the growth rate and the production of a real frequency. Furthermore, many theoretical and simulation results have shown that the equilibrium temperature gradient plays an important role in the evolution of the drift-tearing mode.

The driving mechanism of the electron temperature gradient was first predicted by kinetic theories.[4,5] Later, fluid theory[13] also predicted this result by including the collisional nature of the driven mode, where the thermal force term and an extra parallel force term proportional to the time derivative of the thermal force were included in the parallel electron momentum equation. A comparison between kinetic theories and fluid theories suggests that the neglect of electron–electron collisions in tearing kinetic theories may lead to an overestimate of the temperature gradient free energy in driving tearing mode. The effects of the temperature gradient have been taken into account in many subsequent studies on drift-tearing mode to study the effects of thermal transport[14] or perturbed bootstrap current[15,16] on the drift-tearing mode.

Cylindrical approximation is usually adopted in the theoretical study of tearing modes in tokamak plasmas, with the assumption that the inverse aspect ratio $\epsilon \equiv a/R$ is small. However, this assumption is generally not well satisfied with realistic discharge parameters. The toroidal effects are significant[17] and mainly reflected in the correction of the equilibrium

Supported by the National MCF Energy R&D Program (Grant Nos. 2018YFE0304100, 2018YFE0311300, and 2017YFE0301300), the National Natural Science Foundation of China (Grant Nos. 11675256, 11675257, 11835016, and 11705275), the Strategic Priority Research Program of Chinese Academy of Sciences (Grant No. XDB16010300), the Key Research Program of Frontier Science of Chinese Academy of Sciences (Grant No. QYZDJ-SSW-SYS016), and the External Cooperation Program of Chinese Academy of Sciences (Grant No. 112111KYSB20160039).
*Corresponding author. Email: wzhang@iphy.ac.cn

magnetic field. The equilibrium toroidal magnetic field becomes inhomogeneous in the radial direction, which increases the free energy of the sheared magnetic field for driving the tearing mode when the safety factor q is fixed. In this letter, toroidal effects on the mode structure and growth rate of the drift-tearing mode are studied through numerical simulation. The stabilizing effect of toroidal geometry is obtained, and the plotted contour lines of perturbed fields show the phenomenon of squeezing toward the stronger magnetic field side in the poloidal section.

Our previous simulation research on the drift-tearing mode was based on a fluid model. However, many kinetic theories[4,5,18,19] and simulations[20–22] have shown that kinetic effects have an important influence on the evolution of tearing modes. The kinetic effects of ions are mainly reflected in the finite Larmor radius effect,[20] Landau damping,[19] the coupling of ion-acoustic waves,[18] the influence of energetic passing or trapping ions in the toroidal geometry,[23] etc. It is known that the ion-acoustic wave and ion Landau damping have a stabilizing effect on the drift-tearing mode. As a preliminary attempt, we briefly analyze the hybrid model for fluid electrons and kinetic ions and obtain the dispersion relation of the drift-tearing mode under the influence of the ion finite Larmor radius (FLR) effects. Then, the numerical solution to the dispersion equation is derived. Compared with the dispersion relation under the fluid model, we can see that the FLR effects of ions also have a stabilizing effect on the drift-tearing mode.

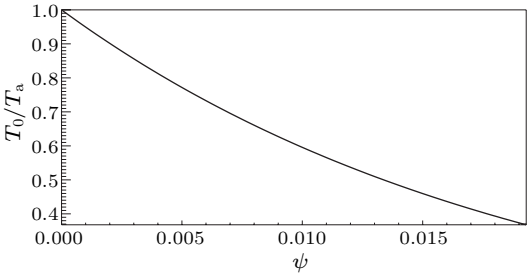

Fig. 1. Radial profile of the equilibrium temperature.

The simulations are carried out with the gyrokinetic toroidal code (GTC), and starting from a previous electromagnetic gyrokinetic model in a toroidal geometry,[24,25] a parallel electron force balance equation was introduced for the simulation of resistive tearing modes[26,27] and drift-tearing modes.[12] In this study, the selected mode numbers are $(m, n) = (2, 1)$ to eliminate the effects of kink coupling. A safety factor profile of $q = 1.5 + 1.2\psi/\psi_w + 0.7(\psi/\psi_w)^2$ is used to contain the $q = 2$ rational surface in the simulation region, where ψ is the poloidal flux, with $\psi = 0$ at the magnetic axis and $\psi = \psi_w$ at the plasma boundary. In order to simulate the drift-tearing mode, a non-uniform equilibrium density distribution of $n_0 = n_a e^{(-\psi/\psi_w)}$ is introduced, where $n_0 = n_{0e} = n_{0i}$, and n_a is the equilibrium on-axis density. Additionally, a nonuniform equilibrium temperature distribution of $T_0 = T_a e^{(-\psi/\psi_w)}$ is introduced to contain the influence of the temperature gradient. Similarly, $T_0 = T_{0e} = T_{0i}$, and T_a is the equilibrium on-axis temperature. The radial profiles of equilibrium temperature are plotted in Fig. 1. The equilibrium on-axis density and temperature are $n_a = 1.0 \times 10^{20}\,\mathrm{m}^{-3}$ and $T_a = 3\,\mathrm{keV}$, respectively. The plasma resistivity is set to a constant value of $\eta = 1.8 \times 10^{-6}\,\Omega{\cdot}\mathrm{m}$, and the magnetic field is $B_0 = 2\,\mathrm{T}$, resulting in $\beta_e = 3\%$, where $\beta_e = 8\pi n_a T_a / B_a^2$ is the plasma on-axis beta for electrons. The inverse aspect ratio is $\epsilon \equiv a/R = 0.3$, where a and R are the minor and major radii of the tokamak device, respectively. The on-axis major radius is set to $R_0 = 1\,\mathrm{m}$.

The temperature gradient can also drive tearing modes as the free energy source, and under the parameters of the present magnetic confinement fusion device, the free energy provided by the equilibrium temperature gradient can be even higher than the free energy contained in the magnetic field shear. According to the previous fluid model,[12] the influence of the temperature gradient on the mode structure and dispersion relation of the drift-tearing mode is studied by adding the equilibrium temperature gradient term to the parallel electron force balance equation,

$$\frac{\partial \delta A_\parallel}{\partial t} = -c\boldsymbol{b}_0 \cdot \nabla \delta\phi + c\eta e n_{0e} \delta u_\parallel + \frac{cT_0}{en_0}\boldsymbol{b}_0 \cdot \nabla \delta n + \frac{cT_0}{en_0}\frac{\delta \boldsymbol{B}}{B_0} \cdot \nabla n_0 + \frac{c(1+\alpha)}{e}\frac{\delta \boldsymbol{B}}{B_0} \cdot \nabla T_0. \quad (1)$$

The last term on the right-hand side is the first-order perturbation term of the temperature gradient in the parallel direction, where $\alpha = 0.71$,[13,28] which represents the correction of thermal force to the temperature gradient term caused by collisions. It should be noted that the energy equation is not included in our fluid model, so the evolution of perturbation temperature is unable to be calculated under this model frame. Therefore, the term related to perturbation temperature is ignored in the electron force balance equation. This will lead to differences in the dispersion relation from other theoretical and simulation results, especially in the real frequency.

The mode structure of the (2,1) drift-tearing mode with the equilibrium temperature gradient by simulation is shown in Fig. 2, with the contours of $\delta\phi$ and $\delta A_\parallel$ on the poloidal cross section and the corresponding radial profile at $\theta = 0$. All the curves are normalized to their maximum absolute values. In the simulations, only mode numbers of $m = 2$ and $n = 1$ are retained; other modes are filtered out via Fourier transformation. The shape of the mode structure is similar to the simulation results without the temperature gradient,[12] but the width of the radial profile is wider.

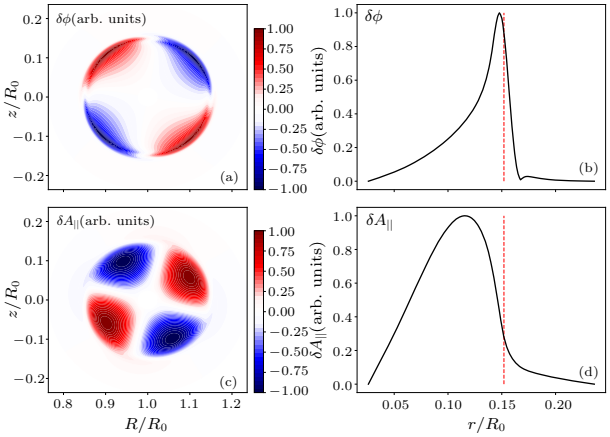

Fig. 2. Mode structure of the $(m, n) = (2, 1)$ drift-tearing mode on the poloidal plane and in the radial direction. (a) and (c) The contours of the perturbed electrostatic potential $\delta\phi$ and the perturbed vector potential $\delta A_\parallel$ on the poloidal cross-section, respectively. (b) and (d) The radial profile of $\delta\phi$ and $\delta A_\parallel$, respectively. The red dashed lines in panels (b) and (d) indicate the position of the $q = 2$ rational surface.

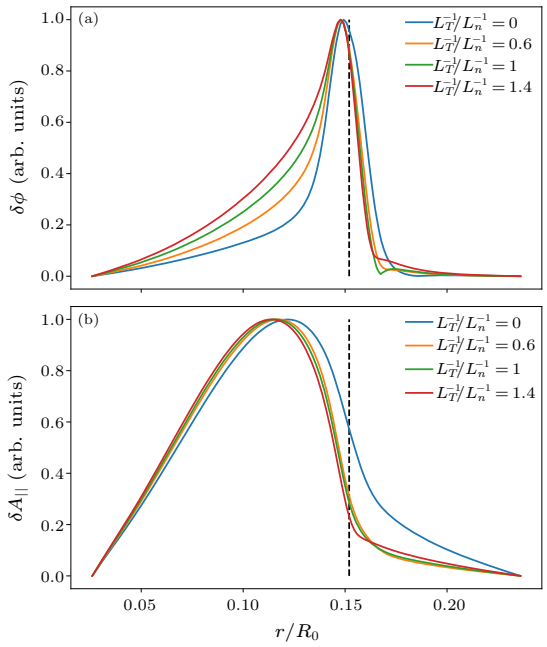

Fig. 3. Radial distribution of (a) perturbed electrostatic potentials $\delta\phi$ and (b) perturbed vector potentials $\delta A_\parallel$ with four different L_T^{-1}/L_n^{-1} values (0, 0.6, 1.0 and 1.4). The black dashed lines indicate the position of the $q = 2$ rational surface.

To study the influence of different equilibrium temperature gradients on the mode width, we scanned four different values of the temperature gradient with a fixed equilibrium density gradient, $L_T^{-1}/L_n^{-1} = 0, 0.6, 1.0, 1.4$, and the radial profiles of these groups of perturbed electrostatic potentials $\delta\phi$ and perturbed parallel vector potentials $\delta A_\parallel$ are plotted in one figure for intuitive comparison, as shown in Fig. 3. The radial mode width of the perturbed electrostatic potential increases with the increase in the temperature gradient. The radial mode width of the perturbed vector potential does not change significantly with the temperature gradient, but their overall profiles move to the left slightly compared with the case of uniform temperature, corresponding to the variation of the perturbed current near the rational surface.

Table 1. The relationship between the growth rate and real frequency of the (2,1) drift-tearing mode with the equilibrium temperature gradient.

L_T^{-1}/L_n^{-1}	0.6	0.8	1.0	1.2	1.4	1.6
Growth rate (10^4 s^{-1})	0.76	1.07	1.44	1.97	2.68	3.45
Frequency (10^4 Hz)	6.72	6.34	5.61	4.73	3.82	2.90

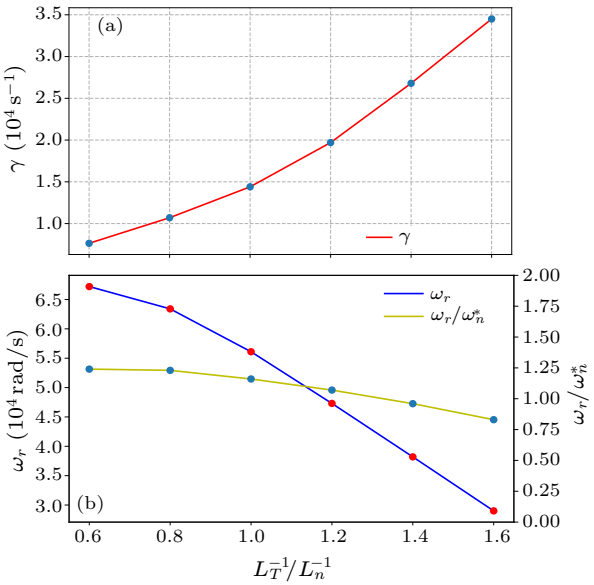

Fig. 4. The relationship between (a) the growth rate and (b) real frequency of the (2,1) drift-tearing mode with values of $L_T^{-1}/L_n^{-1} = 0.6, 0.8, 1.0, 1.2, 1.4, 1.6$.

Then, the influence of different temperature gradient values on the dispersion relation of the drift-tearing mode is studied. We scan six different values of temperature gradient with a fixed density gradient, $L_T^{-1}/L_n^{-1} = 0.6, 0.8, 1.0, 1.2, 1.4, 1.6$. The growth rate and real frequency obtained from the simulation are listed in Table 1, and the relationship curves are plotted according to the data in the table, as shown in Fig. 4. It can be seen that the growth rate of the drift-tearing mode increases with the increase in the temperature gradient. In contrast to the stabilizing effects of the density gradient, the temperature gradient can be an additional driving source of tearing modes. On the other hand, the real frequency decreases with the increase in the temperature gradient, which is different from the theoretical prediction[13] considering the evolution of perturbed temperature. The reason is that the related term of the perturbed temperature is ignored in our GTC fluid model, which results in the loss of the correction of the temperature diamagnetic frequency ω_T^* to the real frequency of the tearing mode. At the same time, to eliminate other physical processes that are significantly affected by the temperature magnitude during the scanning of

temperature gradient, it is necessary to keep a fixed equilibrium temperature at the magnetic axis. Thus, the temperature gradient corresponds to a drop in the local equilibrium temperature at the position of the rational surface, and the local diamagnetic frequency decreases accordingly. The simulated frequency of the drift-tearing mode generally corresponds to the diamagnetic frequency at the position of the rational surface, which is the reason for the decrease in frequency.

The effects of the toroidal geometry are reflected in the geometric modification of the equilibrium magnetic field. The second-order correction term of the magnetic field in the toroidal geometry is retained:

$$B_\zeta = \left[1 - \frac{r}{R_0}\cos\theta + \left(\frac{r}{R_0}\right)^2 \cos^2\theta\right] B_{\zeta 0}, \qquad (2)$$

where r is the coordinate in the direction of the minor radius, and R_0 is the major radius on-axis. The modification of the toroidal effect increases the radial shear of the toroidal magnetic field B_ζ. Since the safety factor q is kept constant in our simulation, the radial shear of the poloidal magnetic field B_θ, that is, the free energy for driving the tearing mode, is also increased.

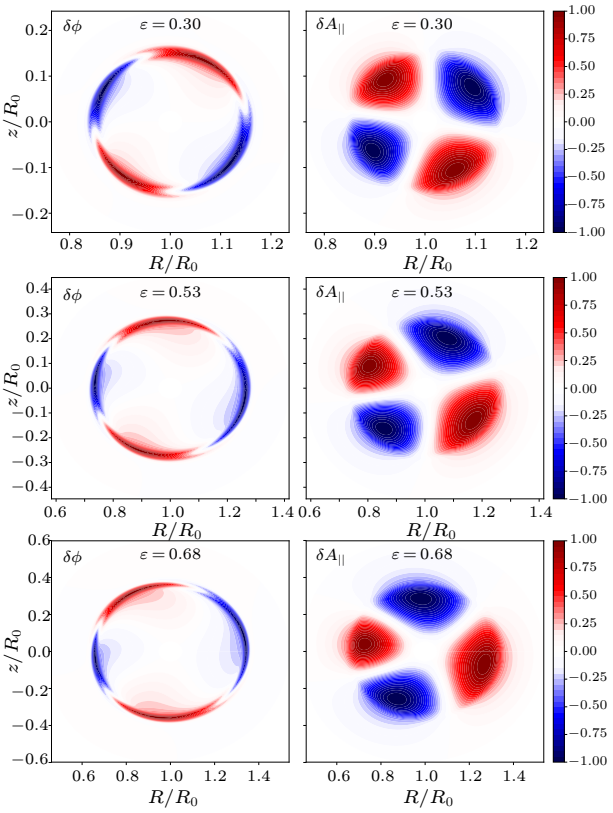

Fig. 5. The distributions of the perturbed potentials $\delta\phi$ and the perturbed vector potentials $\delta A_{||}$ of the drift-tearing mode on the poloidal plane at different aspect ratios ($\epsilon = 0.30, 0.53, 0.68$).

To study the influence of toroidal effects on the mode structure and growth rate of the drift-tearing mode with different inverse aspect ratios, we scanned five different values of inverse aspect ratios ($\epsilon = 0.30, 0.43, 0.53, 0.61, 0.68$), and the simulation is carried out with a constant equilibrium temperature gradient. The profiles of the perturbed electrostatic potentials $\delta\phi$ and the perturbed parallel vector potentials $\delta A_{||}$ on the poloidal plane are obtained, as shown in Fig. 5. The mode structures in the poloidal plane change significantly compared with the simulation result of the cylindrical geometry. The contour lines of both the perturbed electrostatic potentials $\delta\phi$ and the perturbed parallel vector potentials $\delta A_{||}$ show the phenomenon of "squeezing" toward the side of the stronger magnetic field (left side) and the breaking of symmetry. The squeezing phenomenon becomes more serious with the increase in the value of the inverse aspect ratio, indicating that the toroidal effects become more pronounced.

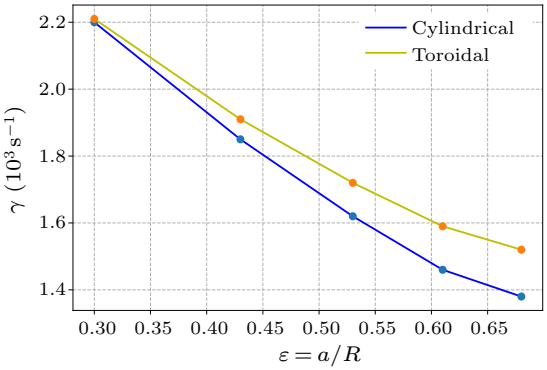

Fig. 6. The relationship between the growth rate of the (2,1) drift-tearing mode with the values of the inverse aspect ratio ($\epsilon = 0.30, 0.43, 0.53, 0.61, 0.68$) in both cylindrical geometry and toroidal geometry.

The growth rates of the drift-tearing mode are calculated from simulation results under five different values of inverse aspect ratios, as shown in Table 2. The relationship curves in the cylindrical geometry and the toroidal geometry are plotted according to the data in the table, as shown in Fig. 6. From the figure, the following conclusions can be made: (i) For the same value of the inverse aspect ratio, the growth rate of the drift-tearing mode in the toroidal geometry is larger than that in the cylindrical geometry, which is due to the increase in the radial shear of the magnetic field, that is, the increase in the free energy of the magnetic field caused by the toroidal modification of the equilibrium magnetic field. (ii) For the same magnetic geometry, when the equilibrium pressure gradient is kept constant, the growth rate of the drift-tearing mode decreases with the increase in the inverse aspect ratio. This is because the major radius of the torus is fixed, and a larger inverse aspect ratio means a larger minor radius. This corresponds to the widening of the radial profile of the safety factor, which leads to a smaller radial shear of the magnetic field. That is to say, the free energy for driving the resistive tearing mode is reduced. (iii) The influence of toroidal effects on the

growth rate of the drift-tearing mode increases with the increase in the inverse aspect ratio, and the reason is that the toroidal effects become more pronounced when the inverse aspect ratio is larger.

Table 2. The relationship between the growth rate of the (2,1) drift-tearing mode with the values of the aspect ratio in both cylindrical geometry and toroidal geometry.

ϵ	0.30	0.43	0.53	0.61	0.68
$\gamma_{\rm cylindrical}$ $(10^3\,{\rm s}^{-1})$	4.21	3.54	3.10	2.80	2.64
$\gamma_{\rm toroidal}$ $(10^3\,{\rm s}^{-1})$	4.23	3.66	3.30	3.04	2.91
Variance	0.5%	3.4%	6.4%	8.6%	10.3%

Ion FLR effects on the dispersion relation of the drift-tearing mode are studied through a simplified analysis of the hybrid model of fluid electrons and kinetic ions in GTC. The details of the hybrid model for drift-tearing mode have been described in Ref. [12]. Assume that the perturbed parallel current is mainly contributed by electrons, i.e., $\delta J_{e\parallel} \gg \delta J_{i\parallel} \simeq 0$. The cylindrical geometry ($\nabla B_0 = 0$) is adopted and then the electron continuity equation and Ampère's law become:

$$\frac{\partial \delta n_e}{\partial t} + B_0 \boldsymbol{b}_0 \cdot \nabla\left(\frac{n_{0e}\delta u_{\parallel e}}{B_0}\right) + B_0 \boldsymbol{v}_E \cdot \nabla\left(\frac{n_{0e}}{B_0}\right) + \delta \boldsymbol{B} \cdot \nabla\left(\frac{n_{0e} u_{\parallel 0e}}{B_0}\right) + \frac{c\nabla \times \boldsymbol{B}_0}{B_0^2} \cdot (-\nabla \delta p_{\parallel e} + n_{0e} \nabla \delta\phi) = 0, \quad (3)$$

$$\nabla_\perp^2 \delta A_\parallel = -\frac{4\pi}{c} \delta J_{\parallel e}. \quad (4)$$

Referring to Drake and Lee's article,[5] only the radial ion polarization drift and $E \times B$ drift with the correction of finite Larmor radius effect are considered. Then, the ion perturbed density is obtained as follows:

$$\delta n_i = \delta n_{i,\rm pol} + \delta n_{i,\delta E\times B} = \frac{c^2}{v_A^2}\frac{1}{4\pi e}\nabla_\perp^2 \delta\phi + k_{\rm Di}^2 \frac{\omega_i^*}{\omega}(1 + \rho_i^2 \nabla_\perp^2)\frac{\delta\phi}{4\pi e}, \quad (5)$$

where $k_{\rm Di}$ is the ion Debye length, and ω_i^* is the ion diamagnetic frequency. Equations (3)–(5) combine the quasi-neutral condition $\delta n_i = \delta n_e$ and the generalized Ohm's law[12] to form a closed system. The dispersion relation for drift-tearing mode can be obtained after some derivations:

$$\omega(\omega + \omega_i^*)(\omega - \omega_e^*)^3 = i\gamma_c^5, \quad (6)$$

where γ_c is the growth rate of the resistive tearing mode, ignoring the pressure gradient. The ω_i^* factor in brackets reflects the ion FLR effects on the drift-tearing mode.

Assume $\omega^* = \omega_e^* = \omega_i^*$. The dispersion equations are solved numerically by scanning the values of γ_c and ω^*. Then, the calculation results of growth rates are compared with the corresponding fluid results. The scanning results in Fig. 7 show that the ion FLR effects have a stabilizing effect on the drift-tearing mode. The physical explanation is that the correction of the finite Larmor radius effect to the ion perturbed $E \times B$ drift causes ions to generate additional radial perturbed velocity, promotes radial energy transport, and eventually leads to the reduction of free energy for driving the drift-tearing mode.

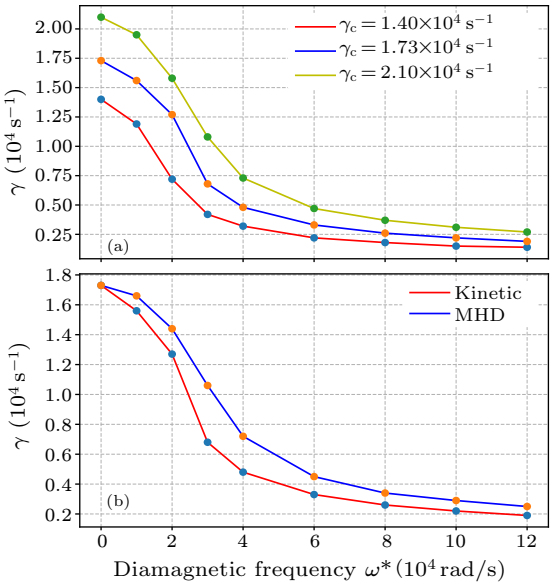

Fig. 7. Numerical solutions of the growth rates of drift-tearing mode under the hybrid model (a), and the results comparison between hybrid model and fluid model (b).

In summary, the effects of the equilibrium temperature gradient, toroidal geometry and ion finite Larmor radius (FLR) on the drift-tearing mode are studied. After introducing the thermal force term into the parallel electron force balance equation, the equilibrium temperature gradient can cause a significant increase in the growth rate of the drift-tearing mode and a broadening of the mode structure. The relation between the real frequency of the drift-tearing mode and the value of the temperature gradient is different from the theoretical prediction that considered the evolution of perturbed temperature. This is due to the neglect of the evolution of perturbation temperature in our model. In the future, we intend to add the energy equation to the system to study the effects of the perturbed temperature on the dispersion relation of the drift-tearing mode.

Toroidal effects on the drift-tearing mode are studied by modifying the toroidal equilibrium magnetic field to the form of toroidal geometry, which increases the radial shear of the magnetic field, i.e., the free energy for driving the drift-tearing mode. Simulation results show that the toroidal effects increase the growth rate of the drift-tearing mode, and the contours of the perturbation field "squeeze" toward the stronger field side in the poloidal section.

Finally, the ion finite Larmor radius (FLR) effects on the dispersion relation of the drift-tearing mode are

briefly studied by analyzing the hybrid model for fluid electrons and kinetic ions, and the corresponding dispersion relation of the drift-tearing mode is obtained. The difference between our dispersion equation and previous kinetic theory[4,5] comes from the neglect of various collision processes in our model, which will be among our future research interests. Then, the numerical solution of the dispersion equation is derived. The numerical solutions are compared between the hybrid model and fluid model, and the results show that the ion FLR effects have a stabilizing effect on the drift-tearing mode.

This research used resources of the National Supercomputer Center in Tianjin (NSCC-TJ), the Oak Ridge Leadership Computing Facility at Oak Ridge National Laboratory (OLCF) and the National Energy Research Scientific Computing Center (NERSC).

References

[1] Furth H P, Killeen J and Rosenbluth M N 1963 *Phys. Fluids* **6** 459
[2] Furth H P, Rutherford P H and Selberg H 1973 *Phys. Fluids* **16** 1054
[3] Rutherford P H 1973 *Phys. Fluids* **16** 1903
[4] Hazeltine R D, Dobrott D and Wang T S 1975 *Phys. Fluids* **18** 1778
[5] Drake J F and Lee Y C 1977 *Phys. Fluids* **20** 1341
[6] Biskamp D 1978 *Nucl. Fusion* **18** 1059
[7] Monticello D A and White R B 1980 *Phys. Fluids* **23** 366
[8] Ye M F, Zhang B Z, Jiang D Y and Li Y N 1998 *Chin. Phys. Lett.* **10** Suppl. p 191
[9] Yang W, Li D and Xu X Q 2018 *Chin. Phys. Lett.* **35** 065201
[10] Xu T, Hu Q M, Hu X W and Yu Q Q 2011 *Chin. Phys. Lett.* **28** 095202
[11] Ji X Q, Yang Q W, Liu Y, Zhou J, Feng B B and Yuan B S 2010 *Chin. Phys. Lett.* **27** 065202
[12] Shi H, Zhang W, Feng H, Lin Z, Dong C, Bao J and Li D 2019 *Phys. Plasmas* **26** 092512
[13] Hassam A B 1980 *Phys. Fluids* **23** 2493
[14] Nishimura S, Yagi M, Itoh S I, Azumi M and Itoh K 2007 *J. Phys. Soc. Jpn.* **76** 064501
[15] Yu Q, Günter S and Scott B D 2003 *Phys. Plasmas* **10** 797
[16] Yu Q 2010 *Nucl. Fusion* **50** 025014
[17] Li D and Huo Y P 1998 *Chin. Phys. Lett.* **10** Suppl. p 154
[18] Bussac M, Edery D, Pellat R and J L S 1978 *Phys. Rev. Lett.* **40** 1500
[19] Connor J, Ham C, Hastie R and Zocco A 2019 *J. Plasma Phys.* **85** 905850204
[20] Chen Y, Chowdhury J, Parker S E and Wan W 2015 *Phys. Plasmas* **22** 042111
[21] Cai H and Fu G 2012 *Phys. Plasmas* **19** 072506
[22] Hornsby W A, Migliano P, Buchholz R, Kroenert L, Weikl A, Peeters A G, Zarzoso D, Poli E and Casson F J 2015 *Phys. Plasmas* **22** 022118
[23] Cai H, Wang S, Xu Y, Cao J and Li D 2011 *Phys. Rev. Lett.* **106** 075002
[24] Holod I, Zhang W L, Xiao Y and Lin Z 2009 *Phys. Plasmas* **16** 122307
[25] Deng W, Lin Z and Holod I 2012 *Nucl. Fusion* **52** 023005
[26] Liu D, Zhang W, Mcclenaghan J, Wang J and Lin Z 2014 *Phys. Plasmas* **21** 122520
[27] Feng H, Zhang W, Dong C, Cao J and Li D 2017 *Phys. Plasmas* **24** 102125
[28] Scott B D, Drake J F and Hassam A B 1985 *Phys. Rev. Lett.* **54** 1027